

RESEARCH ARTICLE

Beaching model for buoyant marine debris in bore-driven swash

Benjamin Davidson^{1,*} , Jamie Brenner¹  and Nimish Pujara¹ 

¹Department of Civil and Environmental Engineering, University of Wisconsin - Madison, Madison, WI 53706, USA

*Corresponding author. E-mail: bmdavidson2@wisc.edu

Received: 25 April 2023; **Revised:** 9 August 2023; **Accepted:** 26 September 2023

Keywords: Particle/fluid flow; Swash flow; Ocean processes; Marine debris

Abstract

Marine debris pollution is a growing problem impacting aquatic ecosystems, coastal recreation and human society. Beaches are known to be a sink for debris, and beaching needs to be accounted for in marine debris mass balances, but the process of buoyant debris beaching is not yet sufficiently well understood in order for it to be included in coastal models. We develop a simplified model for buoyant marine debris transport in bore-driven swash (where swash refers to the area that the water wets the beach with each incoming wave). We validate the model with laboratory experiments and use the combined results from the model and experiments to understand the parameters that are important for dictating particle beaching. The most relevant parameters are the particle inertia and the initial conditions with which debris particles enter the swash zone.

Impact Statement

The fate and transport of buoyant marine debris depend on the fundamentals of particle transport in wave-driven water flow. Particle size and density difference with the water complicate its transport, with further complexities coming from the unsteady nature of swash flows with alternative wetting and drying of the beach. We formulate and test a buoyant marine debris beaching model that accurately predicts beaching and includes the minimal set of processes to do so. This simple beaching model will facilitate improved modelling of buoyant debris transport in the coastal region, which is necessary for analysing marine debris mass budgets and for informing beach clean ups.

1. Introduction

It is no surprise that plastics are the largest component of global marine litter given that plastic waste generation is still increasing, and is likely to continue to increase with the current trends of plastic consumption (Geyer, Jambeck, & Law, 2017). In one year it is estimated that 11 % of plastic waste can make its way into marine environments (Borrelle et al., 2020). Some unknown fraction of that plastic debris collects on shorelines around the world (Rosevelt, Los Huertos, Garza, & Nevins, 2013), with some trends pointing to more marine debris accumulation nearer to population centres (Galgani, Hanke, & Maes, 2015). In studies of marine debris sampled on beaches, plastics often dominate across all debris sizes and beach locations (Compa, Alomar, Morató, Álvarez, & Deudero, 2022; Eriksson, Burton, Fitch, Schulz, & van den Hoff, 2013; Haseler et al., 2020; Ríos et al., 2018). From an aggregate



of almost 1500 publications concerning aquatic debris pollution globally, macro-debris (larger than 5 mm) on beaches has been shown to be mostly plastic, and micro-debris (smaller than 5 mm) was found to be almost entirely composed of plastics (Tekman et al., 2023). Beaches are clearly collection sites for marine debris, but the collection rate and efficiency is currently unknown.

Due to the vast size and dynamic nature of oceanic circulation, numerical models are an effective tool for understanding plastic debris fate and transport throughout the marine environment. Effective models must account for debris sources and sinks, including debris–shoreline interaction and beaching. Hinata, Sagawa, Kataoka, and Takeoka (2020) develop a probabilistic plastic beaching model based on the fluxes of deposited and suspended plastics with the particle residence time on the beach. However, this model focuses on the drift of particles onto the beach from the near shore without much consideration for turbulent processes from wave breaking. Other current models of plastic debris have focused on medium-to-large-scale debris dynamics with poorly defined beaching, with some ignoring debris beaching altogether (van Sebille, England, & Froyland, 2012). For example, Neumann, Callies, and Matthies (2014) did not consider beaching but rather considered the shoreline to be a reflective boundary. Jalón-Rojas, Wang, and Fredj (2019) note that there are many beaching criteria that could be chosen and include a parameter for particles to wash off the beach. Guerrini, Mari, and Casagrandi (2022) assume particle beaching with no resuspension if the entire velocity field at the particle is zero. A common approach across multiple models concerning particle deposition is to consider a particle potentially beached if that particle is in a computational cell along the coast (Atwood et al., 2019; Collins & Hermes, 2019; Kaandorp, Dijkstra, & van Sebille, 2020; Lebreton, Egger, & Slat, 2019; Lebreton, Greer, & Borrero, 2012). This spatial beaching parameter is sometimes accompanied by a requirement for the particle to be stagnant for some duration of time, which Mansui, Molcard, and Ourmières (2015) use as their beaching parameter. Since particle beaching occurs in the swash zone (the region between maximum wave run-up and draw-down) that is shoreward of the surf zone (the region of wave breaking), the current spatial and temporal beaching parameters are problematic. The resolution of these models is usually of the order of kilometres, orders of magnitude larger than the characteristic length scales of the surf and swash zones. Clearly, coarse-resolution models require an improved and more accurate parameterization of beaching based on a better understanding of particle-scale dynamics.

There have been a number of laboratory experiments investigating near shore particle transport and beaching. In the context of wind and wave forcing, Forsberg, Sous, Stocchino, and Chemin (2020) saw buoyant particles mainly deposited on the beach after reaching a steady state under regular waves. In contrast, Kerpen et al. (2020) found buoyant plastics to be distributed nearly equally between the beach and water surface after continuous wave forcing. Núñez, Romano, García-Alba, Besio, and Medina (2023) investigated the fate of particles whether originating on or offshore for many plastic types and shapes, and across various wave conditions; they found particles more dense than water to accumulate in the wave breaking region and particle less dense to accumulate close to shore. Larsen et al. (2023) measured the time it took for microplastic particles to beach given various starting conditions and empirically modelled the particle transport.

While these experiments begin to uncover the mechanisms of buoyant plastic beaching, the physical dynamics leading to the particle deposition on the beach is still unclear. Sediment transport models, like those from Harada, Gotoh, Hiroyuki, and Khayyer (2019a) and Harada, Ikari, Khayyer, and Gotoh (2019b), might be adapted to model the transport of plastic particles that are sized of the order of magnitude of the local sediments. However, plastic debris size is typically an order of magnitude larger than the sediment grain size, which limits the applicability of sediment transport models with debris transport.

In this work, we consider the deposition of buoyant debris on a shallow beach using a combination of mathematical modelling and laboratory experiments. Debris beaching occurs in the swash zone which is driven by breaking waves, also known as bores (Chardón-Maldonado, Pintado-Patiño, & Puleo, 2016). Solitary waves are one way to experimentally generate a bore-driven swash event without the need to consider the impacts of previous or subsequent waves. Investigations of swash zone dynamics

and sediment transport with solitary waves are extensive (Alsina, Falchetti, & Baldock, 2009; Barnes, O'Donoghue, Alsina, & Baldock, 2009; Pujara, Liu, & Yeh, 2015; Sumer et al., 2011) and solitary waves are known to have properties akin to wind-driven waves (Madsen, Fuhrman, & Schäffer, 2008). The 'free swash event' produced by a solitary wave reduces the complexity of the problem yet remains relevant as the particle will be deposited on the beach during the portion of the run-up. We investigate how a debris particle becomes beached during the course of a swash cycle, while accounting for the particle motion as it transitions into the swash zone. We find the velocity of the particle relative to the bore celerity, the lag of the particle behind the bore front and the particle inertia to be important parameters for particle beaching. We show with the proposed model that beaching is more common for particles with higher inertia and for those that enter the swash zone closer to the bore front in time and speed.

In § 2, we develop the particle motion model for buoyant disks in the swash zone, specifically considering particle beaching. We explore the parameters influencing particle fate in regard to deposition on the beach. This model is compared with accompanying laboratory experiments in § 3. Finally, we explore how the forces on buoyant particles dictate beaching in the context of experimental and model results, including the sensitivity of the model results to its input parameters in § 4. We offer brief concluding remarks in § 5.

2. Model

2.1. Equation of particle motion for inertial floating disks in the swash zone

We consider the forces acting on an inertial, floating, disk-shaped particle during a single wave swash event on an inclined slope using a framework from Maxey and Riley (1983). The work from Maxey and Riley (1983) has been expanded to include a free surface with regular waves by Rumer, Crissman, and Wake (1979). The regular wave free surface model has been further expanded to consider the object motion to be driven by gravity (Calvert et al., 2021; Huang, Huang, & Law, 2016; Shen & Zhong, 2001) where the particle slides down the slope of a surface wave in a reference frame that rotates with the wave motion. The work from Maxey and Riley (1983) has been separately expanded to include a free surface and surface current by Beron-Vera, Olascoaga, and Miron (2019). Under bore-driven swash, the slope of the free surface is small (Meyer & Taylor, 1972), so we maintain an inertial reference frame and consider the particle motion to be driven by the swash flow current similar to Beron-Vera et al. (2019).

Figure 1(a) shows the model and experimental set-up with the piston-type wave maker, the plane, impermeable beach at an angle $\tan \theta = 1/10$, the undisturbed wave characteristics and the run-up and draw-down wave profiles. The undisturbed, floating disk-shaped particle is depicted in figure 1(b) with diameter D_p , height H_p , submerged height H_{pw} and height above the water surface H_{pa} . Figure 1(c,d) shows the particle during run-up and draw-down, respectively. We choose a disk-shaped particle with a single aspect ratio, which can represent a range of non-idealized, but highly oblate (flattened) debris shapes that are common for plastics in the environment (Rosal, 2021; Voth & Soldati, 2017). Additionally, the disk shape simplifies the analysis significantly compared with the sphere considered previously (Beron-Vera et al., 2019) since the submerged particle depth is linearly proportional to the volume of water displaced. We define an x - z coordinate system whose origin is at the undisturbed shoreline with x pointing horizontally towards the shore and z vertically upwards. Considering only the forces on the particle from the water (and ignoring forces from the air), we formulate a particle equation of motion that considers the particle to be in vertical equilibrium and subject to forces in the horizontal direction.

During the wave run-up, the particle does not touch the beach (figure 1c) and remains in vertical equilibrium where the mass of the particle (m_p) is equal to the mass of the fluid displaced by the particle (m_f). Once the water depth decreases below H_{pw} at equilibrium, the particle makes contact with the beach; when the particle touches the bottom (figure 1d), the mass equivalency no longer holds since there is an additional reaction force with the beach. For later use in the horizontal momentum balance,

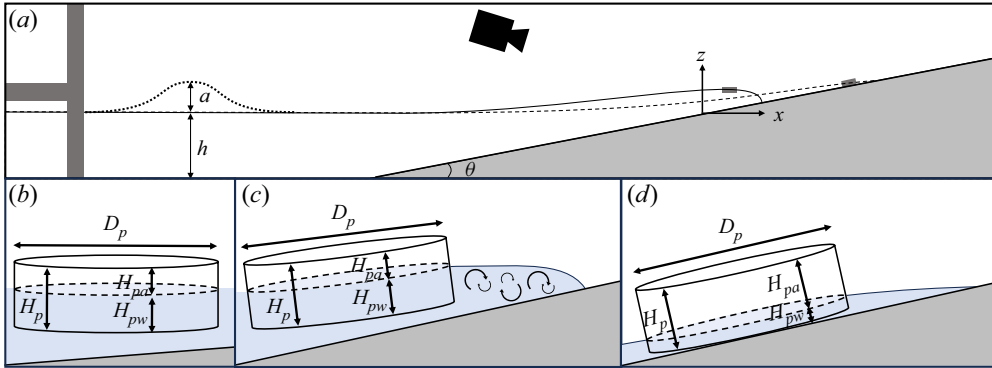


Figure 1. (a) Definition sketch of the incident wave and resulting swash flow acting on the plane beach with an oblique overhead camera. The solid line indicates the water profile during the wave run-up, the dashed line indicates the water profile during run-down and the dotted line indicates the offshore wave profile. The coordinate origin is noted where the still water surface contacts the beach. (b) The undisturbed particle floats with the submergence ratio equal to the density ratio. (c) During the wave run-up, the particle is drawn to the swash tip and remains freely floating due to the depth at the bore front. (d) During the wave draw-down, the depth of the water can decrease below the free floating H_{pw} , and the particle makes contact with the bottom surface.

we consider the ratio of the mass of the fluid displaced to the mass of the particle

$$\frac{m_f}{m_p} = \frac{\rho}{\rho_p} \frac{\pi}{4} \frac{D_p^2 H_{pw}}{D_p^2 H_p} = \frac{\phi}{\gamma}, \tag{2.1}$$

where ρ_p is the particle density, ρ is the fluid density, γ is the particle to fluid density ratio and $\phi = H_{pw}/H_p$ is the particle submergence ratio. Equation (2.1) is unity when the particle weight is completely opposed by buoyancy and zero when the particle weight is completely opposed by the reaction force with the beach. Critically, $\phi = \gamma$ when the particle is floating (figure 1c), and $\phi \neq \gamma$ when the water depth is too shallow for the particle to completely float (figure 1d).

For the particle motion up the beach, we consider the acceleration in the x -direction, which is different to the direction up the slope of the beach by a factor of $\cos \theta$. Because the angle θ tends to be small, the difference between the horizontal and beach-parallel directions is negligible. Consider that $\cos \theta = 1 - \frac{1}{2}\theta^2 + O(\theta^4)$ and $\tan \theta = \theta + O(\theta^3)$ for small θ . Using $s = \tan(\theta)$ to define the slope, we see that $\cos \theta \approx 1$ with a leading-order error of $\frac{1}{2}s^2$. For a beach slope of $s = 1/10$, this leading-order error is 5×10^{-3} and thus is negligibly small.

The swash flow drives the particle motion. Here, we employ a one-way coupled equation to model the particle motion, which is justified since the particle is small compared with the typical swash run-up lengths and the disturbance of the flow from the particle is of second-order importance (Balachandar & Eaton, 2010; Maxey & Riley, 1983). The horizontal forces on the particle are due to fluid forcing, added mass, drag force and frictional force with the beach. This is expressed dimensionally as

$$m_p \frac{dv'_p}{dt'} = m_f \frac{Du'}{Dt'} + C_m m_f \left(\frac{Du'}{Dt'} - \frac{dv'_p}{dt'} \right) - C_D \frac{1}{2} \rho |v'_p - u'| (v'_p - u') D_p H_{pw} + [F'_F], \tag{2.2}$$

where v'_p is the velocity of the particle, u' is the fluid velocity, C_m is the coefficient of added mass, C_D is the coefficient of drag, F'_F is the force of friction with the beach (only acting when the water depth is sufficiently small that the particle makes contact with the beach) and $D/Dt = \partial/\partial t + u\partial/\partial x$ is the

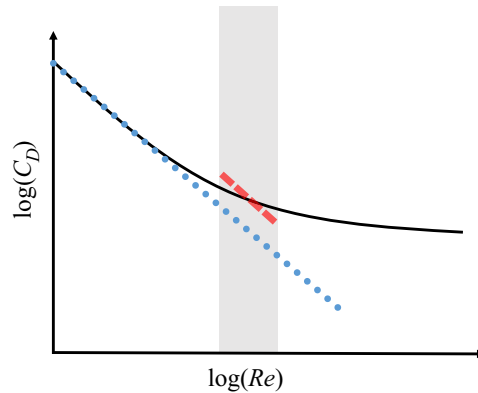


Figure 2. The black line indicates the coefficient of drag as a function of the Reynolds number for a particular shape. The blue dotted line is the Stokes drag approximation for low Re and the red dashed line is the intermediate Re approximation.

material derivative. Here, we note that the v'_p, u', t' and F'_F are dimensional variables as indicated by the prime notation.

We divide (2.2) by m_p using (2.1) and simplify to isolate the particle acceleration. We let the acceleration due to friction be $a'_F = F'_F/m_p$. We address the frictional acceleration fully in § 2.2. We also define a Reynolds number of the flow by the particle slip velocity and particle diameter as $Re = |v'_p - u'|D_p/\nu$. The resulting equation for the particle acceleration is

$$\frac{dv'_p}{dt'} = \left(\frac{\phi + C_m\phi}{\gamma + C_m\phi} \right) \frac{Du'}{Dt'} - \left(\frac{1}{\gamma + C_m\phi} \right) \frac{2C_D\phi\nu}{\pi D_p^2} Re(v'_p - u') + [a'_F]. \tag{2.3}$$

The drag coefficient for a cylindrical disk is a function of Re . The solid, black line in figure 2 sketches this function over a range of Re (Clift, Grace, & Weber, 2013). The dotted blue line indicates the Stokes drag model, $C_D = 13.6/Re$ for a circular disk oriented such that its axis of symmetry is parallel to the flow (Happel & Brenner, 1983). The Stokes model does not well represent the true value of C_D in the shaded region, which is the intermediate Re regime that is typical of a swash flow. Similar to DiBenedetto, Clark, and Pujara (2022), we approximate C_D in the intermediate Re regime as inversely proportional to Re with a new, unknown proportionality constant, C , noted by the dashed red line in figure 2. We substitute C_D for the intermediate Re regime into (2.3) to get

$$\frac{dv'_p}{dt'} = \beta \frac{Du'}{Dt'} - \frac{(v'_p - u')}{\tau_p} + [a'_F], \tag{2.4}$$

where

$$\beta = \frac{\phi + C_m\phi}{\gamma + C_m\phi}; \quad \tau_p = \frac{\pi D_p^2(\gamma + C_m\phi)}{2C\phi\nu}. \tag{2.5a,b}$$

Here, β represents the strength of the fluid forcing and added mass of the fluid acting on the particle, and τ_p represents the relaxation time for the particle in the flow. The unknown empirical coefficient in the drag formulation, C , is absorbed into the particle time scale. We also note that when the water is deep enough such that the particle is freely floating, we can show that $\beta = 1$ from (2.1).

In a swash flow event, the relevant scales of motion are the initial shoreline velocity (U_s) and gravity (g). Using these scales to make (2.4) dimensionless, we define the dimensionless variables $u = u'/U_s$,

$v_p = v'_p/U_s$, $t = t'/(U_s/g)$ and $a_F = a'_F/g$. This gives

$$\frac{dv_p}{dt} = \beta \frac{Du}{Dt} + \frac{(u - v_p)}{St} + [a_F], \tag{2.6}$$

where the particle Stokes number is given by

$$St = \frac{g\tau_p}{U_s}. \tag{2.7}$$

In (2.6), the fluid forcing and the added mass force are captured in the first term, and the drag of the fluid on the particle is captured in the second term.

In addition to the equation for particle motion, we use a classical model for swash flow (Peregrine & Williams, 2001; Shen & Meyer, 1963). For a given beach slope s , the shoreline position, shoreline velocity, flow velocity field and water depth are given by

$$x_s = t - \frac{1}{2}st^2, \tag{2.8a}$$

$$u_s = 1 - st, \tag{2.8b}$$

$$u = \frac{1}{3} \left(1 - 2st + 2\frac{x}{t} \right), \tag{2.8c}$$

$$h = \frac{1}{9} \left(1 - \frac{1}{2}st - \frac{x}{t} \right)^2, \tag{2.8d}$$

where $x_s = x'_s/(U_s^2/g)$ is the dimensionless shoreline position, $u_s = u'_s/U_s$ is the dimensionless shoreline velocity, $u = u'/U_s$ is the dimensionless fluid velocity and $h = h'/(U_s^2/g)$ is the dimensionless water depth. This bore-driven swash model has been shown to accurately describe the flow evolution in a single swash event in laboratory experiments (see figures 19–20 corresponding to surging and plunging breaker in Pujara et al., 2015). Thus, the model of swash flow accurately captures the flow evolution in a swash event, but does not necessarily account for other complexities in the swash zone such as infragravity waves or swash interaction between waves.

2.2. Extra considerations for beaching particles

We supplement (2.6) to capture aspects of particle motion in the swash zone that are critical, but not included in the dynamics so far. Specifically, we account for the dynamics of the swash tip where debris particles will collect. We also consider the frictional force on the particle with the beach when the water depth goes to zero.

The swash tip is typically a blunt edge (figure 1c) due to the effects of friction and flow convergence (Baldock, Grayson, Torr, & Power, 2014; Pujara, Liu, & Yeh, 2016), which will collect debris particles during the wave run-up. However, this is not captured in the flow model. To account for particle motion in the swash tip, we first define the particle location (x_p) relative to the shoreline location (x_s) as

$$\xi = x_s - x_p. \tag{2.9}$$

We then make two modifications to the swash model. The first is that during the run-up, we expect the depth of the water near the swash tip to be greater than the particle since friction creates a ‘blunt nose’ at the tip. Using the definition of β from (2.5a,b), we make the simplification that $\beta = 1$ throughout the wave run-up. Second, we implement a spatial dependency on the Stokes number during the run-up,

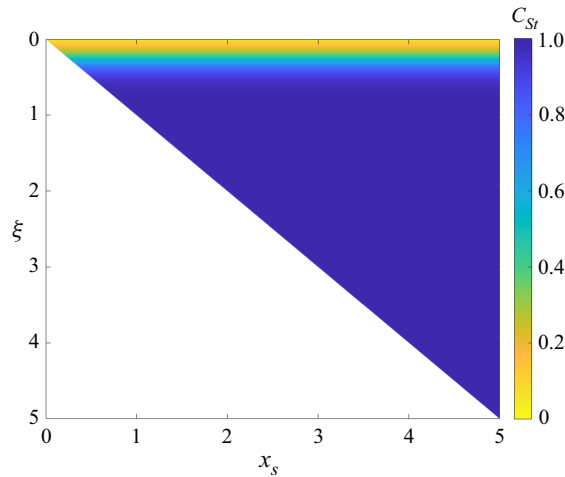


Figure 3. The Stokes number coefficient (C_{St}) during the wave run-up, shown as a function of the particle position relative to the shoreline (ξ) and the shoreline position (x_s); C_{St} decreases for a particle near the shoreline, while a particle far from the shoreline is unaffected. The Stokes coefficient noticeably deviates from unity in the region of approximately 1/10 of the maximum run-up.

which accounts for the fact that the particle becomes more tracer-like in the fast and turbulent swash tip

$$St_{eff} = C_{St}St = \frac{1}{1 + \exp(-k(\xi - w))} St. \quad (2.10)$$

Here, the coefficient C_{St} ranges from 0 to 1, acting to decrease the effective Stokes number in the vicinity near the tip during the wave run-up, which is essentially a boundary layer to the swash flow. The constant k represents a sharpness factor that determines how smoothly the C_{St} varies with ξ , and w determines the width of the zone where the C_{St} noticeably falls below unity. While the results presented below are not sensitive to the precise values, using $k = 10$ and $w = 0.25$ provides an effective region of approximately 1/10 of the maximum run-up where the Stokes number is modified (figure 3). The swash tip size (10% of the maximum run-up) is an approximation, but consistent with previous data and models of the swash tip (Baldock et al., 2014; Pujara et al., 2016).

On the wave draw-down, we consider the particle to be prone to beaching if it is left behind by the fluid and the local water depth at the particle becomes zero. In reality, the particle will make contact with the beach and the solid body friction force will be non-zero before the beach is completely dry (figure 1d). However, we assume that the flow dynamics will be more important than the lubricated friction force until the water depth reaches zero and as such can be neglected. Once the local water depth at the particle goes to zero, there is no buoyant force on the particle and the particle's weight is only balanced by the reaction force from the beach. In the x -direction, there is no longer any force from the fluid and the only force on the particle is the friction force acting opposite to its direction of motion. We model this friction force using the standard formulation $F_F = \mu N = \mu m_p g$, where μ is the coefficient of friction between the particle and the beach. In the absence of water, the deceleration of the particle due to friction is then given by

$$a_F = -\mu \operatorname{sgn}(v_p). \quad (2.11)$$

2.3. Model results

We solve the full model, (2.6) with the spatially dependent Stokes number (2.10) and the optional friction acceleration term (2.11) with MATLAB using a standard solver (*ode45*). The model parameters

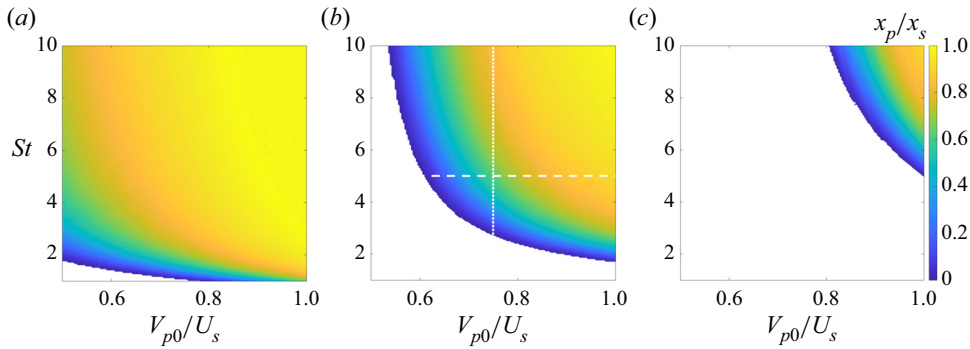


Figure 4. Fraction of final particle location over maximum shoreline run-up, for beaching particles as a function of particle Stokes number (St) and dimensionless initial particle velocity (V_{p0}/U_s) at three dimensionless initial particle times: (a) $t_{p0}/(2U_s/(gs)) = 0.001$, (b) $t_{p0}/(2U_s/(gs)) = 0.01$, (c) $t_{p0}/(2U_s/(gs)) = 0.1$, where $2U_s/(gs)$ is the duration of the swash event. The dotted and dashed white lines indicate transects considered in figure 5.

including γ , C_m , μ and H_p are chosen for the case of the experimental particles in § 3. The particle begins moving at $(x, t) = (0, t_{p0})$ with an initial velocity $v(x = 0, t = t_{p0}) = V_{p0}$. Initializing the model in this way also serves to avoid the singularity in the flow velocity, depth and acceleration which are undefined at $(x = 0, t = 0)$.

We show the impact of particle inertia and initial conditions on the beaching dynamics in figure 4. The figure shows the final location of the particle at the given conditions. After a particle is returned to the water, the model is no longer accurate and the final location is left blank as the particle is not deposited on the beach. We consider Stokes numbers in the range $St \in [1, 10]$, which is a realistic range considering that it covers $\tau_p \in [0.2, 2]$ s for a swash event with $U_s = 2 \text{ m s}^{-1}$. For the particle’s initial velocity, we consider the range $V_{p0}/U_s \in [0.5, 1]$. While the lower limit is an arbitrary choice, the upper limit corresponds physically to a particle that is caught in the bore front. Apart from the initial velocity, the initial time at which the particle enters the swash zone is also important. The initial dimensionless time of the particle crossing $x = 0$, $t_{p0}/(2U_s/(gs)) = [0.001, 0.01, 0.1]$ relates to the distance the particle is behind the swash tip at the start of the run-up. For the smaller dimensionless zero-crossing time, the particle is closer to the bore front.

Although we treat them separately in figure 4, we note that the initial particle velocity and time are likely to be correlated such that a particle that enters the swash later is likely to do so at a lower velocity. Additionally, we expect the particle St and the initial conditions to be related as the particle inertia likely dictates motion in the surf zone and thus the resulting initial conditions.

As expected, the likelihood of particle beaching increases at higher St . This is because at higher St , the particle does not change direction as quickly as the water. The water drains before the particle can respond, leaving the particle beached. We also observe that particles are more likely to beach when they enter the swash zone at a higher initial velocity. The larger initial velocity causes the particle to stay near the swash tip, reach closer to the maximum wave run-up, and become deposited on the beach during the downrush. When a particle enters the swash close behind the swash tip, we see that it is very likely to be beached (figure 4a). In this case, the beaching location is also very sensitive to St . When a particle enters the swash far behind the swash tip, it is far less likely to be beached (figure 4c). The particle will only beach in this case if it is very inertial and has a large initial velocity. Under the intermediate initial time (figure 4b) beaching depends on both St and the initial particle velocity, which we explore further in figure 5.

Figure 5(a) shows the particle trajectories from figure 4(b) with $V_{p0}/U_s = 0.75$ and varied St . We see that, across this range of St , the particle trajectory and final particle location change significantly. Similarly, figure 5(b) shows the particle trajectories from figure 4(b) with $St = 5$ with varied initial

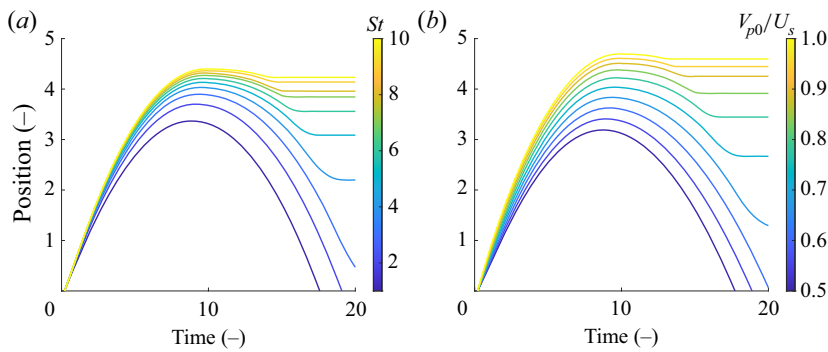


Figure 5. Model particle trajectories at transects from figure 4 with one varied parameter. (a) Transect at the vertical dotted line in figure 4(b) showing varied St . (b) Transect at the horizontal dashed line in figure 4(b) showing varied dimensionless velocity.

particle velocities. We again see that the particle trajectory and resultant beaching location change significantly. Overall, whether a particle is beached and the location where it is beached is quite sensitive to the particle's swash Stokes number and its initial conditions as it enters the swash.

3. Experiments

3.1. Wave flume experiments

We performed particle beaching experiments in the Water Science and Engineering Laboratory wave flume at the University of Wisconsin - Madison. The wave flume is 39 m long, 0.91 m wide and 1.12 m tall. We use a piston-type wave maker to generate a solitary wave (Goring, 1978) that acts incident to a 1/10 sloped impermeable, plane beach shown in figure 1(a). The generated wave has an amplitude of 0.06 m at the still water depth of 0.3 m ($a/h = 0.2$). This wave incident on the specified beach produces a surging-type breaking wave (Grilli, Svendsen, & Subramanya, 1997).

We place five, three-dimensionally printed polypropylene plastic disks just offshore of the beach, near the still water line. The particles have measured diameters of 2.261 ± 0.002 cm, heights of 0.268 ± 0.003 cm and masses of 0.819 ± 0.002 g. The average density is 0.760 ± 0.008 g cm⁻³.

We use an obliquely mounted overhead digital camera with a frame rate of 30 f.p.s. to capture the swash event and particle motion. Throughout the camera field of view (figure 6), are calibration marks which are used to convert the particle location in pixels to distance in laboratory coordinates. We track the particle trajectories and shoreline motion using custom code written in MATLAB. For particle tracking, we first subtract the image background and binarize the image data based on a threshold that selects the particle. We manually identify the starting location of each particle and for frames after the initial two frames, we find the particle velocity from the particle displacement over the previous two frames to predict the subsequent location of the particle. We use the nearest neighbour algorithm from the predicted location to find the true location of the particle. Figure 6(a) shows the last frame with the trajectory of each particle superimposed.

From the camera images, we also track the shoreline position which is clearly observed by the sharp wet/dry boundary of the wavefront moving up the beach seen in figure 6(b,c). We manually track the shoreline motion during the uprush by selecting the maximum run-up location in each frame.

At the very start of the swash cycle, the shoreline motion is obstructed from view by the steepness of the breaking wave as it collapses while passing through $x = 0$. We trim the data to only consider the shoreline motion after the wave bore collapsed and the position of the shoreline could be accurately tracked. However, trimming the shoreline position data means we do not know the time at which the shoreline first moved nor its initial velocity, both of which are needed for the swash model. This

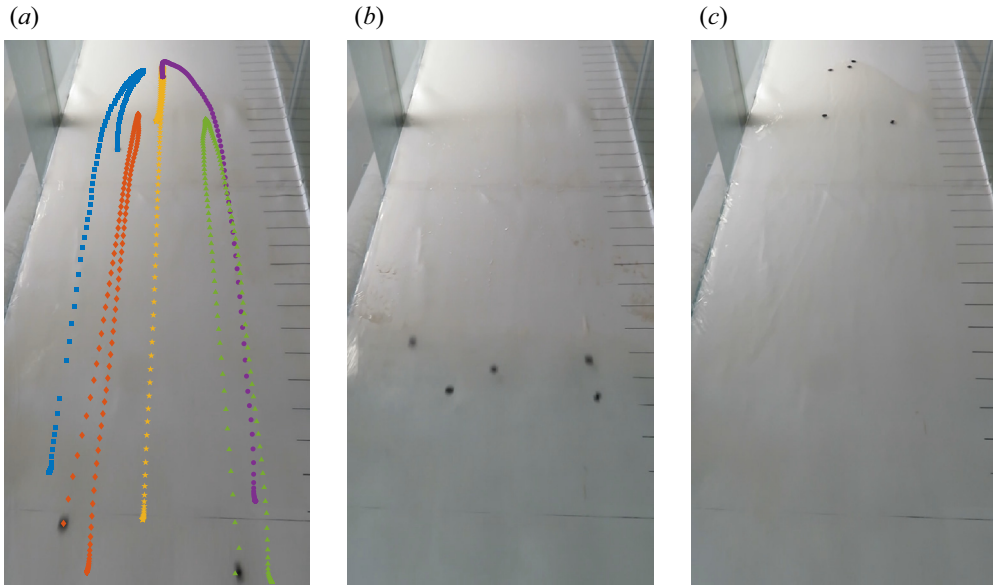


Figure 6. Oblique camera images. (a) Last frame with particle trajectories: particle A, blue squares; particle B, orange diamonds; particle C, yellow stars; particle D, purple circles; and particle E, green diamonds. (b) Sample frame during run-up. (c) Sample frame near maximum run-up.

uncertainty is also related to the physics of bore collapse. The swash solution in (2.8) is based upon the nonlinear shallow water equations, in which the shoreline moves impulsively upon the wave bore arrival at the initial shoreline position. In reality, the wave bore collapse process occurs over some finite time and distance (Pujara et al., 2015; Yeh & Ghazali, 1988). Since the bore collapse is not instantaneous, there is a brief time of shoreline acceleration before a maximum initial shoreline velocity is reached.

From the shoreline position data, we find the shoreline velocity using a Gaussian convolution (Mordant, Crawford, & Bodenschatz, 2004; Ouellette, Xu, & Bodenschatz, 2006) with a filter width of 2 frames and filter support of 7 frames. In our data, we confirm that the maximum observed shoreline velocity occurs at the same time that the wave bore visually appeared completely collapsed. Since we expect the shoreline position after complete bore collapse to follow (2.8a) (at least in the absence of friction), and $t = 0$ is defined as the time at which the wave passes through $x = 0$, we implement a time shift in the shoreline data to account for the finite time of the bore collapse process

$$x_{s,data} = U_s(t - t_0) - \frac{1}{2}gs(t - t_0)^2. \quad (3.1)$$

By fitting a portion of the data from the beginning of the wave run-up after bore collapse to (3.1) using the maximum velocity after the bore collapse as an initial guess for the initial shoreline velocity, we find the initial shoreline velocity to be $U_s = 1.89 \text{ m s}^{-1}$. The shoreline data and model are plotted together in figure 7, where we see that the shoreline model fits the shoreline data well at the start of the uprush. The model predicts a slightly higher maximum run-up than we see in the experimental data, as expected since the shoreline model is frictionless. We do not have experimental shoreline position data during the draw-down because tracking the shoreline location optically becomes near impossible during the draw-down process when there is no longer an obvious demarcation between the dry and wet beach.

The particle data are defined on the same time vector as the shifted shoreline data. To find the exact time and velocity with which each particle crossed the initial shoreline position, t_{p0} and V_{p0} , we fit a

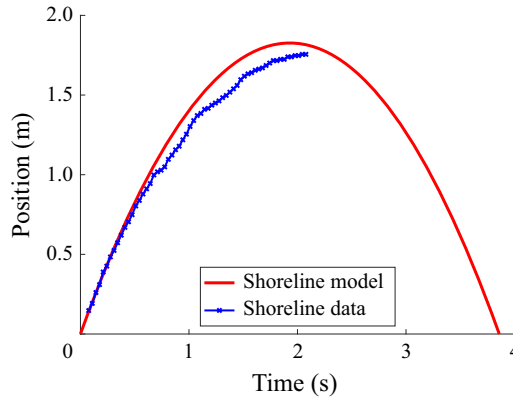


Figure 7. Run-up shoreline data and model fit to (3.1) with an initial shoreline velocity of $U_s = 1.89 \text{ m s}^{-1}$ and a time shift of $t_0 = 0.11 \text{ s}$.

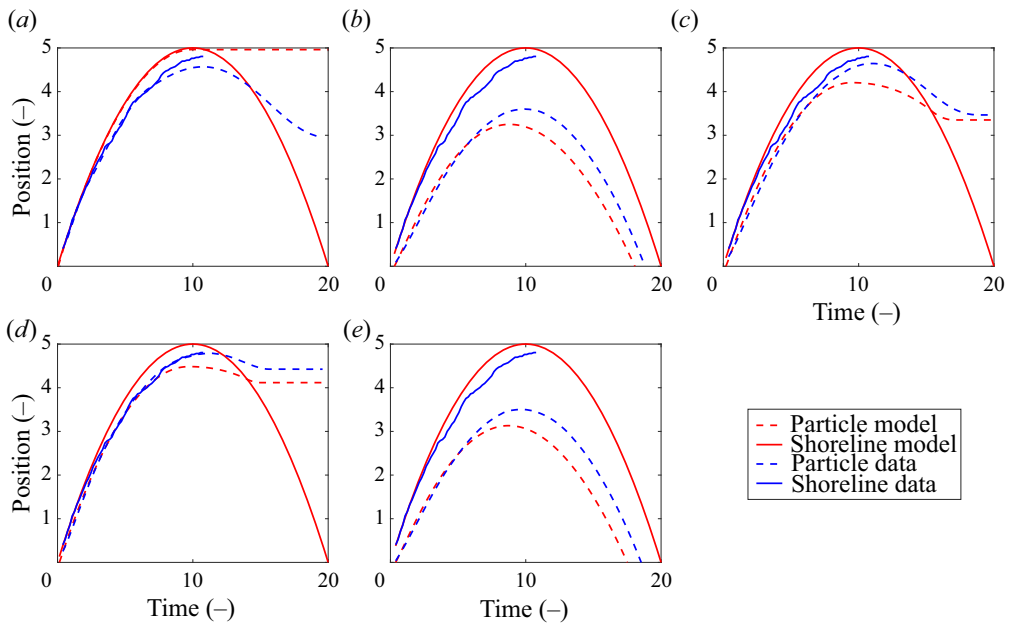


Figure 8. Model and experimental shoreline run-up plotted with model and experimental particle trajectory for five experimental particles with initial conditions listed in table 1. Panels (a–e) correspond to particles A–E, respectively.

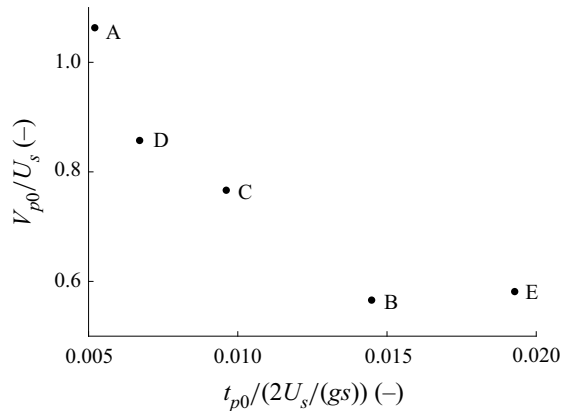
fifth-order polynomial to each particle trajectory and analytically evaluate the zero-crossing time and velocity.

3.2. Experimental particle trajectories and comparison with model

In figure 8 we show the experimental particle and shoreline trajectories with the model particle and shoreline trajectories. Table 1 lists the initial conditions and fate for each particle. The correlation between the particle initial velocity and initial time are shown in figure 9. Generally, a particle that enters the swash zone closer to the wavefront will enter with a greater velocity; a particle that enters the swash zone further behind the wave bore will enter with a lower velocity. Besides the particle initial

Table 1. *Experimental particle initial conditions and fate from figure 8.*

Particle	V_{p0}/U_s	$t_{p0}/(2U_s/(gs))$	Fate
A	1.03	0.0028	beach
B	0.57	0.015	water
C	0.77	0.0096	beach
D	0.86	0.0067	beach
E	0.58	0.019	water

**Figure 9.** *Particle initial velocity vs. initial time. Particles that enter the swash zone closer to the wave will enter with a larger velocity, and those that are further behind the wavefront will enter the swash zone with a lower velocity.*

conditions, the rest of the model parameters are: $\tau_p = 1$ s (corresponding to $St = 5.18$), $\gamma = 0.76 \text{ g cm}^{-3}$, $C_m = 0.75$, $\mu = 0.15$ and $H_p = 0.268$ cm. We choose τ_p as a reasonable order of magnitude estimate of the particle time scale that facilitates agreement between the model and data. The values of γ and H_p are as measured from the experimental particles, and C_m is taken as the average value between the added mass coefficient of a sphere ($C_m = 1/2$) and a circular cylinder ($C_m = 1$) (Newman, 2017). The dynamic friction coefficient for non-metals usually ranges from 0.3 to 0.4 and is lower when moist or well lubricated (Rabinowicz, 1965). From the wetness of the beach surface after a swash event, we justify the estimated friction coefficient of $\mu = 0.15$. We further explore the sensitivity of the model to these predicted values in § 4.

The comparison between the data and model trajectories in figure 8 shows that the model captures the qualitative behaviour observed in the experiments. In particular, the model trajectories correctly predict whether a particle is deposited on the beach (particles A, C and D) or returned to the water (particles B and E) without any case-specific tuning of parameters. Of the beached particles, the location of beaching in the model is also close to the observed value in two of the three beaching particle cases (particles C and D). In each case, the experimental particle trajectories match the model very well at the start of the swash event, with the deviation between the data and the model growing until the time of the maximum run-up.

The shoreline evolves during run-up and does not maintain a uniform alongshore profile. We see at the maximum shoreline run-up, figure 6(c), that the shoreline is further at the spanwise centre of the beach. In addition to the shoreline evolution, we note that in figure 6(a), the particles closer to the edge drift inwards toward the centre of the beach during the run-up. This is especially evident in particles A, D and E. This drift towards the centre in combination with the non-uniform shoreline profile means that

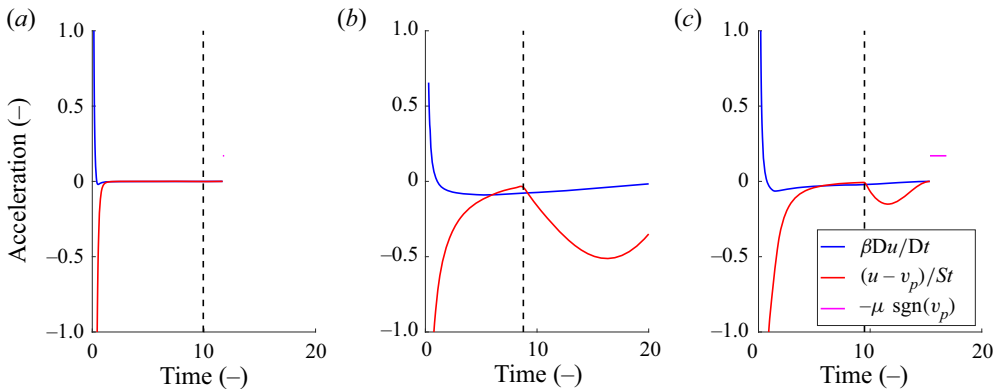


Figure 10. Acceleration components actively contributing to the particle force balance as a function of time for particles A–C from figure 8(a–c), respectively. The dashed black line indicates the point in time where the fluid at the particle location changes direction. We note that there is a small pink region in (a), none in (b) and a larger pink region in (c).

the particles starting at the edges fall further behind the shoreline over time than is accounted for in the model. This phenomenon explains the discrepancy between the beaching locations in the experiments and in the model for particle A.

In figure 8, for particles B–E, the particle trajectory model and data match well during the first third of the swash cycle, but start to deviate near the peak of the trajectory. Given that we have made no attempt to fine tune the particle Stokes number, which is based on an order of magnitude estimate of the particle time scale ($\tau_p = 1$ s), the model can be considered quite robust in terms of capturing the essential particle motion and fate. However, this does point to a need to better understand particle inertia for debris in the swash zone.

Apart from considering the particle trajectories between the model and experiment, another useful comparison is examining the particle trajectory relative to the shoreline, in the experiment and the model. This captures whether the model contains enough physics to predict the particle beaching dynamics. In this regard, we see that the trends of particle behaviour with the shoreline compare very well for all three beaching particles in the experiment and the model. Not only do the model trajectories capture the particle deceleration during uprush that is the result of the complex flow–particle interaction, but they also capture how the particle decelerates to zero velocity as it gets beached. Further, the experimental results confirm the fact that beaching was very sensitive to initial conditions which is consistent with the model results (§ 2.3).

Finally, we consider the acceleration budget of particles A, B and C, in figure 10. Two of these are beaching particles (particle A, deposited high on the beach in the model, and particle C, deposited lower on the beach in the model), and one returns to the water (particle B). At the beginning of each particle’s trajectory, each particle experiences a positive (up the beach) force from the first term in (2.6) and a greater force acting in the opposite, negative (down the beach) direction from the middle term of (2.6). For the particles that eventually beach, these two forces both quickly approach zero during the uprush; this occurs faster for particle A (figure 10a) which is beached close to the maximum run-up. For the particle that returns to the water (particle B, figure 10b), the first and second terms decrease in magnitude slower. After the flow reverses direction at the particle location, noted by the vertical black dashed line, the second term (drag) increases in magnitude. The increased drag force is in the negative direction acting to wash the particle back into the water. We see this slightly in particle C (figure 10c), but the particle runs out of water before it travels sufficiently downslope to return to the main water body, resulting in particle beaching.

Table 2. Model parameters with an estimated range of appropriate values and the resulting range in final particle location. The parameters are listed in descending order of the final particle location range. Here, X notes that the particles were returned to the water.

Parameter	Estimated range	Final location range
s	1/20–1/5	1.5–6.2
V_{p0}/U_s	0.5–1	X–4.6
$t_{p0}/(2U_s/(gs))$	0.001–0.1	X–4.6
St	1–10	X–4.2
H_p	(0.1–0.5) cm	2.0–3.4
μ	0.1–0.5	3.1–3.3
γ	(0.7–0.9) g cm ⁻³	3.1–3.3
C_m	0.5–1	3.1–3.2

4. Discussion

The main free parameters in this model are the particle initial conditions and the particle Stokes number, St . The dimensionless particle initial time and velocity are characteristics of the particle motion from the surf zone into the swash zone; they are consequences of the particle motion within the surf zone and are related as shown in figure 9. The particle Stokes number St is a measure of the particle inertia. We considered the impact of varied St and initial conditions in figures 4 and 5, but now we consider the sensitivity of the model results to all parameters, including C_m , μ , γ , H_p and s . We start by considering a single model particle trajectory with $St = 5$, $V_{p0}/U_s = 0.75$ and $t_{p0}/(2U_s/(gs)) = 0.01$. This trajectory is noted by the intersection of the dotted and dashed lines in figure 4(b). We then solve for the trajectory of this particle while changing individual parameters over a range of reasonable values and examine the spread of the final particle location (table 2). The flow model is only defined for $x > 0$, so particles that return to the water are denoted with a final particle location of X in table 2. The parameters are listed in descending order of importance. We see that the parameters that have the most impact are those already discussed above: the particle initial conditions (t_{p0} , V_{p0}), and the particle inertia (St). An additional significant parameter is the beach slope, which was not varied in these experiments but appears to affect the particle beaching location significantly. The particle height also did not change in the experiments but shows to have a moderate effect on the particle beaching. The impacts from changing μ , γ and C_m are an order of magnitude smaller than the other parameters, thus the estimated values are sufficient for approximating the particle trajectory.

We can also determine in which direction each parameter impacts the particle's beaching location. As already pointed out in figure 4, decreases in the initial time increase the particle location up the beach, while increases in the initial velocity and St both increase the final location of the particle. For the other parameters, the final beaching location increases with increases to H_p , μ and γ , and decreases with increases to slope and C_m .

This model expands the understanding of buoyant particle transport in the swash zone despite its simplicity. In the particle transport model, we use the effective Stokes number and $\beta = 1$ to account for the swash tip during run-up. While the swash zone is characterized by the turbulent mixing of breaking waves, it appears that turbulence is not important for particle beaching in the swash zone at this scale. This is likely because we are considering particles sized of the order of the swash depth, where the force of buoyancy is more important than forcing from turbulent mixing. The result is that beaching is mainly determined by how the mean flow couples to particle inertia. In more realistic scenarios, we also hypothesize that sediment–particle interactions are likely to be less important since the particles are much larger than sediment, but this remains to be tested. Additional research is necessary at the microplastic scale, where the interactions of these particles with sediments and turbulence will likely

play an important role. Concerning the implementation of friction with the beach, we take a simple approach that friction starts once the beach is dry. In reality, as soon as the water depth decreases so the particle is in contact with the beach, the force of friction begins acting on the particle. Accounting for this phenomenon may require a transitional regime where friction with the beach begins before the beach is completely dry at the particle location. Although we make these assumptions and suggest such improvements, these assumptions hold for our simple model, demonstrated by the agreement with the experiments and the analysis in § 3.2.

5. Conclusions

We present a model for buoyant, inertial particle transport in bore-driven swash to understand the factors leading to marine debris beaching. This is not an exhaustive model, but rather a minimal model that includes only the most essential dynamics that can be used to predict particle beaching effectively. We have validated this model with experiments and explored the sensitivity of its results to the parameterizations and assumptions made. The particle initial conditions entering the swash zone and the particle inertia are the most important factors dictating particle fate (i.e. beaching); the particle velocity and location as it enters the swash zone dictate whether the particle is caught up in the swash tip during uprush, while the particle inertia dictates whether the particle will become beached as a result of being unable to change direction and follow the fluid down the slope. At present, this model considers only cross-shore transport and the idealized case of a single-bore-driven swash on a plane beach. Complexities will arise when accounting for oblique waves, multiple bore wave trains, debris of different shapes where the orientation dynamics is important, debris of larger size where lubrication pressures may become important and other environmental factors such as natural beach morphology and wind effects. However, we expect that the essence of the debris-beaching process we have identified will hold regardless of additional parameters and environmental factors.

Supplementary material. All data are available upon request from the corresponding author.

Acknowledgements. We acknowledge fruitful conversations with Gautier Verhille.

Funding statement. We gratefully acknowledge funding from the Freshwater Collaborative of Wisconsin (Grant No. T2-5/20–06).

Declaration of interests. The authors report no conflict of interest.

Author contributions. B.D., J.B. and N.P. developed the model; B.D. and N.P. designed the experiments; B.D. performed the experiments; B.D. wrote the manuscript; N.P. and J.B. provided revisions; N.P. supervised the project.

References

- Alsina, J.M., Falchetti, S., & Baldock, T.E. (2009). Measurements and modelling of the advection of suspended sediment in the swash zone by solitary waves. *Coastal Engineering*, 56, 621–631. <https://doi.org/10.1016/j.coastaleng.2009.01.007>
- Atwood, E.C., Falcieri, F.M., Piehl, S., Bochow, M., Matthies, M., Franke, J., . . . Siegert, F. (2019). Coastal accumulation of microplastic particles emitted from the po river, northern italy: Comparing remote sensing and hydrodynamic modelling with in situ sample collections. *Marine Pollution Bulletin*, 138, 561–574. <https://doi.org/10.1016/j.marpolbul.2018.11.045>
- Balachandar, S., & Eaton, J.K. (2010). Turbulent dispersed multiphase flow. *Annual Review of Fluid Mechanics*, 42, 111–133. <https://doi.org/10.1146/annurev.fluid.010908.165243>
- Baldock, T., Grayson, R., Torr, B., & Power, H. (2014). Flow convergence at the tip and edges of a viscous swash front – Experimental and analytical modeling. *Coastal Engineering*, 88, 123–130. <https://doi.org/10.1016/j.coastaleng.2014.02.008>
- Barnes, M., O’Donoghue, T., Alsina, J., & Baldock, T. (2009). Direct bed shear stress measurements in bore-driven swash. *Coastal Engineering*, 56, 853–867. <https://doi.org/10.1016/j.coastaleng.2009.04.004>
- Beron-Vera, F.J., Olascoaga, M.J., & Miron, P. (2019). Building a Maxey–Riley framework for surface ocean inertial particle dynamics. *Physics of Fluids*, 31(9), 096602. <https://doi.org/10.1063/1.5110731>
- Borrelle, S.B., Ringma, J., Law, K.L., Monnahan, C.C., Lebreton, L., McGivern, A., . . . Rochman, C.M. (2020). Predicted growth in plastic waste exceeds efforts to mitigate plastic pollution. *Science*, 369(6510), 1515–1518. <https://doi.org/10.1126/science.aba3656>

- Calvert, R., McAllister, M., Whittaker, C., Raby, A., Borthwick, A., & van den Bremer, T. (2021). A mechanism for the increased wave-induced drift of floating marine litter. *Journal of Fluid Mechanics*, *915*, A73. <https://doi.org/10.1017/jfm.2021.72>
- Chardón-Maldonado, P., Pintado-Patiño, J.C., & Puleo, J.A. (2016). Advances in swash-zone research: Small-scale hydrodynamic and sediment transport processes. *Coastal Engineering*, *115*, 8–25. <https://doi.org/10.1016/j.coastaleng.2015.10.008>
- Clift, R., Grace, J.R., & Weber, M.E. (2013). *Bubbles, drops, and particles*. Mineola, NY: Dover Publications.
- Collins, C., & Hermes, J. (2019). Modelling the accumulation and transport of floating marine micro-plastics around South Africa. *Marine Pollution Bulletin*, *139*, 46–58. <https://doi.org/10.1016/j.marpolbul.2018.12.028>
- Compa, M., Alomar, C., Morató, M., Álvarez, E., & Deudero, S. (2022). Spatial distribution of macro- and micro-litter items along rocky and sandy beaches of a marine protected area in the western Mediterranean Sea. *Marine Pollution Bulletin*, *178*, 113520. <https://doi.org/10.1016/j.marpolbul.2022.113520>
- DiBenedetto, M.H., Clark, L.K., & Pujara, N. (2022). Enhanced settling and dispersion of inertial particles in surface waves. *Journal of Fluid Mechanics*, *936*, A38. <https://doi.org/10.1017/jfm.2022.95>
- Eriksson, C., Burton, H., Fitch, S., Schulz, M., & van den Hoff, J. (2013). Daily accumulation rates of marine debris on sub-Antarctic island beaches. *Marine Pollution Bulletin*, *66*(1), 199–208. <https://doi.org/10.1016/j.marpolbul.2012.08.026>
- Forsberg, P.L., Sous, D., Stocchino, A., & Chemin, R. (2020). Behaviour of plastic litter in nearshore waters: First insights from wind and wave laboratory experiments. *Marine Pollution Bulletin*, *153*, 111023. <https://doi.org/10.1016/j.marpolbul.2020.111023>
- Galgani, F., Hanke, G., & Maes, T. (2015). Global distribution, composition and abundance of marine litter. In M. Bergmann, L. Gutow, & M. Klages (Eds.), *Marine anthropogenic litter* (pp. 29–56). Cham, Switzerland: Springer International Publishing. https://doi.org/10.1007/978-3-319-16510-3_2
- Geyer, R., Jambeck, J.R., & Law, K.L. (2017). Production, use, and fate of all plastics ever made. *Science Advances*, *3*(7), e1700782. <https://doi.org/10.1126/sciadv.1700782>
- Goring, D.G. (1978). *Tsunamis-The propagation of long waves onto a shelf* (Unpublished doctoral dissertation). California Institute of Technology, Pasadena, CA.
- Grilli, S.T., Svendsen, I.A., & Subramanya, R. (1997). Breaking criterion and characteristics for solitary waves on slopes. *Journal of Waterway, Port, Coastal, and Ocean Engineering*, *123*(3), 102–112. [https://doi.org/10.1061/\(ASCE\)0733-950X\(1997\)123:3\(102\)](https://doi.org/10.1061/(ASCE)0733-950X(1997)123:3(102))
- Guerrini, F., Mari, L., & Casagrandi, R. (2022). A coupled Lagrangian-Eulerian model for microplastics as vectors of contaminants applied to the Mediterranean Sea. *Environmental Research Letters*, *17*(2), 024038. <https://doi.org/10.1088/1748-9326/ac4fd9>
- Happel, J., & Brenner, H. (1983). *Low Reynolds number hydrodynamics: with special applications to particulate media*. The Hague, the Netherlands: Martinus Nijhoff Publishers.
- Harada, E., Gotoh, H., Hiroyuki, I., & Khayyer, A. (2019a). Numerical simulation for sediment transport using mps-dem coupling model. *Advances in Water Resources*, *129*, 354–364. <https://doi.org/10.1016/j.advwatres.2017.08.007>
- Harada, E., Ikari, H., Khayyer, A., & Gotoh, H. (2019b). Numerical simulation for swash morphodynamics by DEM–MPS coupling model. *Coastal Engineering Journal*, *61*(1), 2–14. <https://doi.org/10.1080/21664250.2018.1554203>
- Haseler, M., Balcianas, A., Hauk, R., Sabaliauskaite, V., Chubarenko, I., Ershova, A., & Schernewski, G. (2020). Marine litter pollution in baltic sea beaches – application of the sand rake method. *Frontiers in Environmental Science*, *8*, 599978. <https://doi.org/10.3389/fenvs.2020.599978>
- Hinata, H., Sagawa, N., Kataoka, T., & Takeoka, H. (2020). Numerical modeling of the beach process of marine plastics: A probabilistic and diagnostic approach with a particle tracking method. *Marine Pollution Bulletin*, *152*, 110910. <https://doi.org/10.1016/j.marpolbul.2020.110910>
- Huang, G., Huang, Z.H., & Law, A.W.K. (2016). Analytical study on drift of small floating objects under regular waves. *Journal of Engineering Mechanics*, *142*(6), 06016002. [https://doi.org/10.1061/\(ASCE\)EM.1943-7889.0001067](https://doi.org/10.1061/(ASCE)EM.1943-7889.0001067)
- Jalón-Rojas, I., Wang, X.H., & Fredj, E. (2019). A 3D numerical model to Track Marine Plastic Debris (TrackMPD): Sensitivity of microplastic trajectories and fates to particle dynamical properties and physical processes. *Marine Pollution Bulletin*, *141*, 256–272. <https://doi.org/10.1016/j.marpolbul.2019.02.052>
- Kaandorp, M.L.A., Dijkstra, H.A., & van Sebille, E. (2020). Closing the Mediterranean marine floating plastic mass budget: Inverse modeling of sources and sinks. *Environmental Science & Technology*, *54*(19), 11980–11989. <https://doi.org/10.1021/acs.est.0c01984>
- Kerpen, N.B., Schlurmann, T., Schendel, A., Gundlach, J., Marquard, D., & Hüpgen, M. (2020). Wave-induced distribution of microplastic in the surf zone. *Frontiers Marine Science*, *7*, 590565. <https://doi.org/10.3389/fmars.2020.590565>
- Larsen, B.E., Al-Obaidi, M.A.A., Guler, H.G., Carstensen, S., Goral, K.D., Christensen, E.D., Kerpen, N.B., Schlurmann, T., & Fuhrman, D.R. (2023). Experimental investigation on the nearshore transport of buoyant microplastic particles. *Marine Pollution Bulletin*, *187*, 114610. <https://doi.org/10.1016/j.marpolbul.2023.114610>
- Lebreton, L., Egger, M., & Slat, B. (2019). A global mass budget for positively buoyant macroplastic debris in the ocean. *Scientific Reports*, *9*(1), 12922. <https://doi.org/10.1038/s41598-019-49413-5>
- Lebreton, L., Greer, S., & Borrero, J. (2012). Numerical modelling of floating debris in the world's oceans. *Marine Pollution Bulletin*, *64*(3), 653–661. <https://doi.org/10.1016/j.marpolbul.2011.10.027>
- Madsen, P.A., Fuhrman, D.R., & Schäffer, H.A. (2008). On the solitary wave paradigm for tsunamis. *Journal of Geophysical Research: Oceans*, *113*. <https://doi.org/10.1029/2008JC004932>

- Mansui, J., Molcard, A., & Ourmières, Y. (2015). Modelling the transport and accumulation of floating marine debris in the Mediterranean Basin. *Marine Pollution Bulletin*, 91(1), 249–257. <https://doi.org/10.1016/j.marpolbul.2014.11.037>
- Maxey, M.R., & Riley, J.J. (1983). Equation of motion for a small rigid sphere in a nonuniform flow. *Physics of Fluids*, 26(4), 883. <https://doi.org/10.1063/1.864230>
- Meyer, R.E., & Taylor, A.D. (1972). Run-up on beaches. In R. E. Meyer (Ed.), *Waves on beaches and resulting sediment transport* (pp. 357–411). Academic Press. <https://doi.org/10.1016/B978-0-12-493250-0.50014-X>
- Mordant, N., Crawford, A., & Bodenschatz, E. (2004). Experimental Lagrangian acceleration probability density function measurement. *Physica D: Nonlinear Phenomena*, 193(1–4), 245–251. <https://doi.org/10.1016/j.physd.2004.01.041>
- Neumann, D., Callies, U., & Matthies, M. (2014). Marine litter ensemble transport simulations in the southern North Sea. *Marine Pollution Bulletin*, 86(1–2), 219–228. <https://doi.org/10.1016/j.marpolbul.2014.07.016>
- Newman, J.N. (2017). *Marine hydrodynamics*. Cambridge, MA: The MIT Press.
- Núñez, P., Romano, A., García-Alba, J., Besio, G., & Medina, R. (2023). Wave-induced cross-shore distribution of different densities, shapes, and sizes of plastic debris in coastal environments: A laboratory experiment. *Marine Pollution Bulletin*, 187, 114561. <https://doi.org/10.1016/j.marpolbul.2022.114561>
- Ouellette, N.T., Xu, H., & Bodenschatz, E. (2006). A quantitative study of three-dimensional Lagrangian particle tracking algorithms. *Experiments in Fluids*, 40(2), 301–313. <https://doi.org/10.1007/s00348-005-0068-7>
- Peregrine, D.H., & Williams, S.M. (2001). Swash overtopping a truncated plane beach. *Journal of Fluid Mechanics*, 440, 391–399. <https://doi.org/10.1017/S002211200100492X>
- Pujara, N., Liu, P.L.-F., & Yeh, H. (2015). The swash of solitary waves on a plane beach: Flow evolution, bed shear stress and run-up. *Journal of Fluid Mechanics*, 779, 556–597. <https://doi.org/10.1017/jfm.2015.435>
- Pujara, N., Liu, P.L.-F., & Yeh, H. (2016). An integral treatment of friction during a swash uprush. *Coastal Engineering*, 114, 295–300. <https://doi.org/10.1016/j.coastaleng.2016.04.015>
- Rabinowicz, E. (1965). *Friction and wear of materials*. New York, NY: John Wiley & Sons.
- Ríos, N., Frias, J.P., Rodríguez, Y., Carriço, R., Garcia, S.M., Juliano, M., & Pham, C.K. (2018). Spatio-temporal variability of beached macro-litter on remote islands of the North Atlantic. *Marine Pollution Bulletin*, 133, 304–311. <https://doi.org/10.1016/j.marpolbul.2018.05.038>
- Rosal, R. (2021). Morphological description of microplastic particles for environmental fate studies. *Marine Pollution Bulletin*, 171, 112716. <https://doi.org/10.1016/j.marpolbul.2021.112716>
- Rosevelt, C., Los Huertos, M., Garza, C., & Nevins, H. (2013). Marine debris in central California: Quantifying type and abundance of beach litter in Monterey Bay, CA. *Marine Pollution Bulletin*, 71(1–2), 299–306. <https://doi.org/10.1016/j.marpolbul.2013.01.015>
- Rumer, R.R., Crissman, R.D., & Wake, A. (1979). *Ice transport in great lakes*. Great Lakes Environmental Research Laboratory, National Oceanic and Atmospheric Administration.
- Shen, H.H., & Zhong, Y. (2001). Theoretical study of drift of small rigid floating objects in wave fields. *Journal of Waterway, Port, Coastal, and Ocean Engineering*, 127(6), 343–351. [https://doi.org/10.1061/\(ASCE\)0733-950X\(2001\)127:6\(343\)](https://doi.org/10.1061/(ASCE)0733-950X(2001)127:6(343))
- Shen, M.C., & Meyer, R.E. (1963). Climb of a bore on a beach Part 3. Run-up. *Journal of Fluid Mechanics*, 16(1), 113. <https://doi.org/10.1017/S0022112063000628>
- Sumer, B.M., Sen, M.B., Karagali, I., Ceren, B., Fredsøe, J., Sottile, M., . . . Fuhrman, D.R. (2011). Flow and sediment transport induced by a plunging solitary wave. *Journal of Geophysical Research: Oceans*, 116. <https://doi.org/10.1029/2010JC006435>
- Tekman, M., Gutow, L., Macario, A., Haas, A., Walter, A., & Bergmann, M. (2023). *Alfred-wegener-institut helmholtz-zentrum für polar- und meeresforschung*. Retrieved from https://litterbase.awi.de/litter_graph
- van Sebille, E., England, M.H., & Froyland, G. (2012). Origin, dynamics and evolution of ocean garbage patches from observed surface drifters. *Environmental Research Letters*, 7(4), 044040. <https://doi.org/10.1088/1748-9326/7/4/044040>
- Voth, G.A., & Soldati, A. (2017). Anisotropic particles in turbulence. *Annual Review of Fluid Mechanics*, 49, 249–276. <https://doi.org/10.1146/annurev-fluid-010816-060135>
- Yeh, H.H., & Ghazali, A. (1988). On bore collapse. *Journal of Geophysical Research: Oceans*, 93, 6930–6936. <https://doi.org/10.1029/JC093iC06p06930>